A Platinum Open Access Journal for Organic Chemistry

Paper

Free to Authors and Readers

DOAJ Seal

Arkivoc **2027** (2) 202612638

Heteroatom exchange as a scaffold-editing strategy: a matched xanthone–acridone study of aminoalkyl derivatives

Agustina Gonzalez,[a] A. Paula Irazoqui,[ab] Claudia G. Buitrago,*[ac] and Dario C. Gerbino*[d]

[a] Departamento de Biología, Bioquímica y Farmacia, Universidad Nacional del Sur, San Juan 671, 8000 Bahía Blanca, Argentina. [b] Comisión de Investigaciones Científicas de la Provincia de Buenos Aires (CIC PBA), Argentina. [c] CCT-CONICET, Camino La Carrindanga km 7, 8000 Bahía Blanca, Argentina. [d] Instituto de Química del Sur, INQUISUR (CONICET-UNS). Departamento de Química, Universidad Nacional del Sur. Avenida Alem 1253, 8000 Bahía Blanca, Argentina

Email: cbuitrag@criba.edu.ar dgerbino@uns.edu.ar

Dedicated to Professor Teodoro S. Kaufman in recognition of his outstanding contributions to synthetic organic and heterocyclic chemistry, and for his enduring influence on generations of chemists in Argentina and the international scientific community

Received 06-24-2026 **Accepted** 08-14-2026 **Published on line** 08-20-2026

Abstract

Heteroatom exchange represents a valuable scaffold-editing strategy for property modulation of bioactive heterocyclic systems while preserving overall molecular architecture. In the present study, a matched-scaffold approach was employed to evaluate the contribution of heteroatom identity to the biological responses of closely related aminoalkylated xanthone and acridone derivatives. Both derivatives were comparatively evaluated and the experimental findings indicate that a defined heteroatom replacement within a conserved heterocyclic framework can modulate the properties of closely related scaffolds. More broadly, this study highlights the value of matched xanthone–acridone systems as experimentally accessible models for investigating scaffold-dependent effects and structure–response relationships in heterocyclic chemistry.

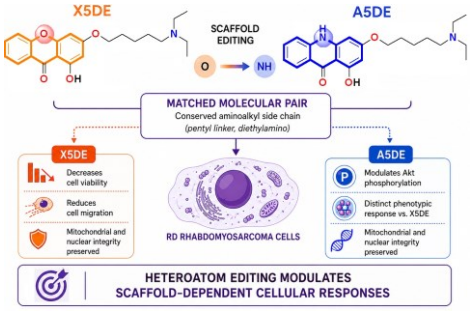

Keywords: Xanthones; acridones; heteroatom exchange; scaffold editing; matched molecular pairs; aminoalkyl derivatives; structure–response relationships

Cite as *Arkivoc* **2027** (2) 202612638

DOI: https://doi.org/10.24820/ark.5550190.p012.638

©AUTHOR(S)

1. Introduction

Xanthones and acridones are two prominent families of dibenzo-fused heterocyclic compounds that have attracted sustained interest owing to their structural diversity, synthetic accessibility, and broad spectrum of biological activities.[1-4] Both scaffolds have served as versatile platforms for the development of antimicrobial, antiparasitic, anti-inflammatory, neuroactive, and antitumoral agents, stimulating extensive efforts toward their synthesis, functionalization, and biological evaluation.[1-4] Structurally, they are closely related tricyclic heteroaromatic systems that differ primarily in the identity of the endocyclic heteroatom, namely oxygen in xanthones and nitrogen in acridones (Figure 1). This seemingly subtle modification alters electronic distribution, hydrogen-bonding properties, polarity, acidity/basicity balance, and tautomeric behavior while preserving the overall molecular topology.[5,6]

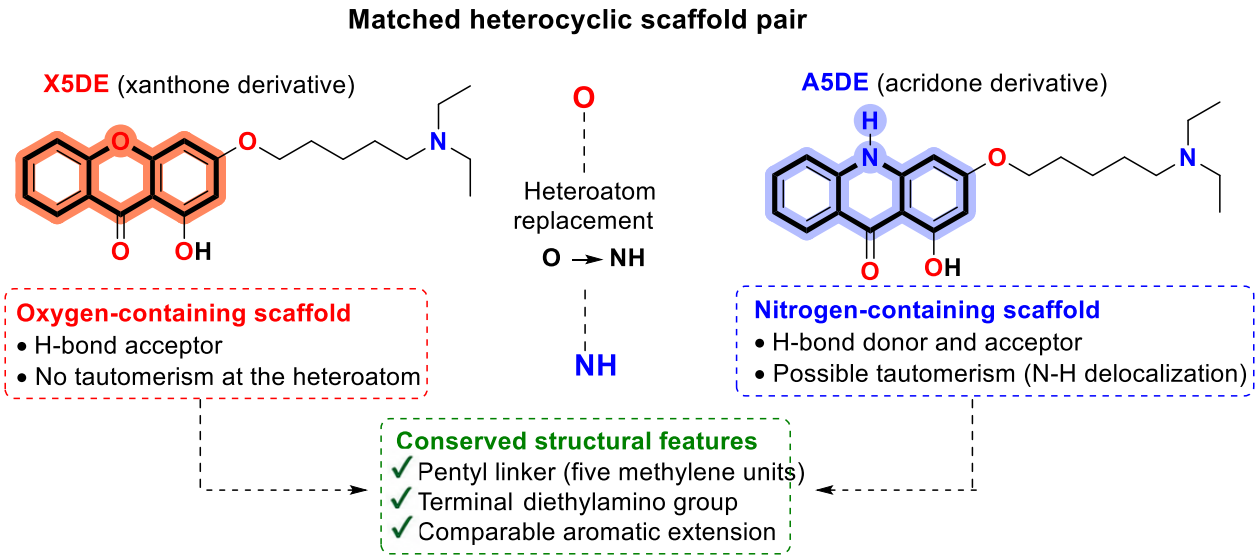

Figure 1. Matched-scaffold design employed in the present study.

Hydroxylated xanthones and acridones are particularly valuable synthetic intermediates because they readily undergo *O*-functionalization and related derivatization reactions, providing efficient access to structurally diverse analogues.[1,2,7,8] Among these, 1,3-dihydroxyxanthone (**1,3-DHX**) and 1,3-dihydroxyacridone (**1,3-DHA**) are especially attractive owing to their conserved substitution patterns, which facilitate direct comparison of closely related derivatives.

As part of our continuing interest in oxygen- and nitrogen-containing heterocyclic systems, we previously reported the synthesis and biological evaluation of aminoalkylated derivatives derived independently from **1,3-DHX** and **1,3-DHA**.[9,10] In the xanthone series, aminoalkyl-substituted derivatives demonstrated the suitability of the 1,3-DHX scaffold for late-stage diversification through *O*-functionalization.[9] Structurally related aminoalkylated acridones derived from **1,3-DHA** were subsequently shown to modulate Akt-associated signaling pathways in skeletal muscle cells.[10] Together, these studies established efficient synthetic access to structurally matched xanthone and acridone derivatives suitable for comparative biological evaluation.

Recent studies have also compared structurally related xanthone and acridone derivatives to investigate the influence of heteroatom identity on biological activity. Santra *et al*. reported matched xanthone–acridone analogues displaying distinct antiproliferative profiles against human cancer cell lines,

 ©AUTHOR(S)

whereas Georgakopoulos *et al*. demonstrated that oxygen-to-nitrogen substitution within closely related heterocyclic frameworks produced measurable differences in physicochemical and biological properties.[11,12] These reports support the concept that heteroatom exchange may influence biological behavior even within highly similar molecular frameworks.

Although comparative studies involving xanthone and acridone derivatives have been reported,[11,12] relatively few have focused specifically on isolating the contribution of a single scaffold modification within a rigorously matched molecular framework. Matched molecular pair strategies provide a rigorous framework for evaluating such discrete structural modifications while minimizing the influence of peripheral substituent effects.[13-16] By varying only one structural element, these approaches enable direct assessment of the molecular and biological consequences associated with a defined scaffold modification.

The present study examines the biological properties of two structurally matched aminoalkyl derivatives, **X5DE** and **A5DE**, derived from **1,3-DHX** and **1,3-DHA**, respectively (Figure 1). Both derivatives preserve identical aminoalkyl substitution patterns, linker architecture, and terminal diethylamino functionality, differing only in the identity of the endocyclic heteroatom within the tricyclic scaffold. Accordingly, this work was designed as a scaffold-comparison study rather than a conventional structure–activity relationship investigation, allowing direct evaluation of how a single heteroatom exchange influences the biological properties of closely related xanthone and acridone derivatives within a rigorously defined molecular framework.

2. Results and Discussion

2.1 Chemistry

The matched xanthone–acridone compounds evaluated in this study, **X5DE** and **A5DE**, were prepared by the synthetic procedures previously developed by our group.[9,10] These synthetic routes are summarized in Scheme 1, and complete experimental procedures and spectroscopic characterization are provided in the Experimental Section.

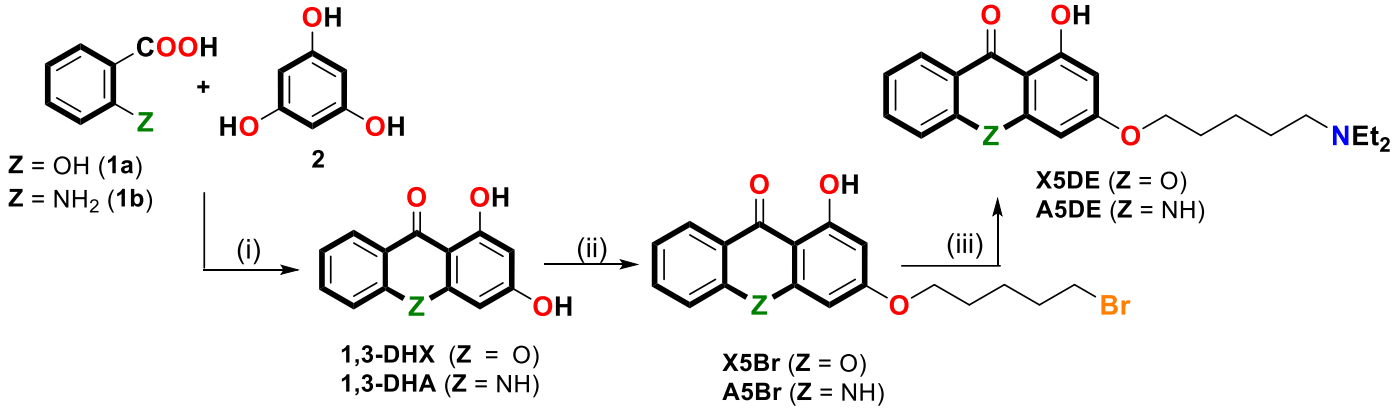

Scheme 1. Synthetic access to the aminoalkylated xanthone and acridone derivatives **X5DE** and **A5DE**. Reagents and conditions: (i) preparation of **1,3-DHX** and **1,3-DHA** according to previously reported procedures; (ii) 1,5-dibromopentane, K_2CO_3, acetone, room temperature (**X5Br**) or reflux (**A5Br**); (iii) diethylamine, acetone, room temperature (**X5DE**); diethylamine, room temperature (**A5DE**).

 ©AUTHOR(S)

Preparation of **X5DE** started from **1,3-DHX**, previously synthesized by the cyclocondensation methodology reported by our group.[9] Selective *O*-alkylation with 1,5-dibromopentane afforded the bromopentyl intermediate **X5Br**, which subsequently underwent nucleophilic substitution with diethylamine to furnish the target aminoalkylated xanthone derivative **X5DE**.

An analogous synthetic sequence was employed for the preparation of **A5DE**. The corresponding precursor, **1,3-DHA**, was prepared according to our previously reported methodology,[10] followed by *O*-alkylation with 1,5-dibromopentane to give intermediate **A5Br**. Subsequent nucleophilic substitution with diethylamine afforded the aminoalkylated acridone derivative **A5DE**.

Although **X5DE** and **A5DE** were previously reported independently,[9,10] their direct comparison as a structurally matched xanthone–acridone pair has not been investigated. The identity of all intermediates and final compounds was confirmed by ^{1}H and ^{13}C NMR spectroscopy, FT-IR spectroscopy, and HRMS. The spectroscopic data were in agreement with the proposed structures and with those previously reported for these compounds.[9,10] Copies of the corresponding spectra are provided in the Supporting Information.

2.2 Biological comparison of structurally matched xanthone–acridone derivatives

The biological evaluation of **X5DE** and **A5DE** was performed to investigate the influence of scaffold identity on cellular responses in rhabdomyosarcoma (RMS and C2C12 myoblast)-associated models. Considering that both derivatives constitute a chemically matched xanthone–acridone pair, the experimental design was not intended to establish a conventional structure–activity relationship (SAR) based on extensive analogue generation, but rather to evaluate the biological consequences associated with a defined heteroatom exchange within a conserved molecular framework.

The selection of complementary biological assays was aimed at providing a comparative characterization of the cellular responses induced by both scaffolds, including effects on cell viability, long-term proliferative capacity, migration-associated behavior, and selected molecular markers related to cellular signaling. Since linker architecture and terminal amine functionality were maintained constant, differences observed between **X5DE** and **A5DE** were interpreted in the context of the contribution of the xanthone or acridone core.

Previous studies have demonstrated that aminoalkylated xanthone and acridone derivatives may interact with relevant cellular pathways and display distinct biological profiles depending on their structural features.[9,10] Therefore, the present comparative approach provides a controlled framework to examine how replacement of the endocyclic oxygen atom by a nitrogen functionality influences the biological response profile of closely related heterocyclic systems.

2.2.1 Comparative effects of X5DE on the viability of RMS cells and C2C12 myoblasts. Trypan blue exclusion assays, a widely used method for assessing cell viability based on plasma membrane integrity,[17] were initially performed to comparatively evaluate the effects of **X5DE** on cell viability in RD rhabdomyosarcoma cells and C2C12 myoblasts. Treatment with **X5DE** (1.0 µM) significantly reduced the number of viable RD cells after both 24 and 48 h, whereas the viability of C2C12 myoblasts remained largely unaffected under the same experimental conditions (Figure 2). These results indicate a differential cellular response to the xanthone derivative between transformed and non-transformed muscle-derived cells.

 ©AUTHOR(S)

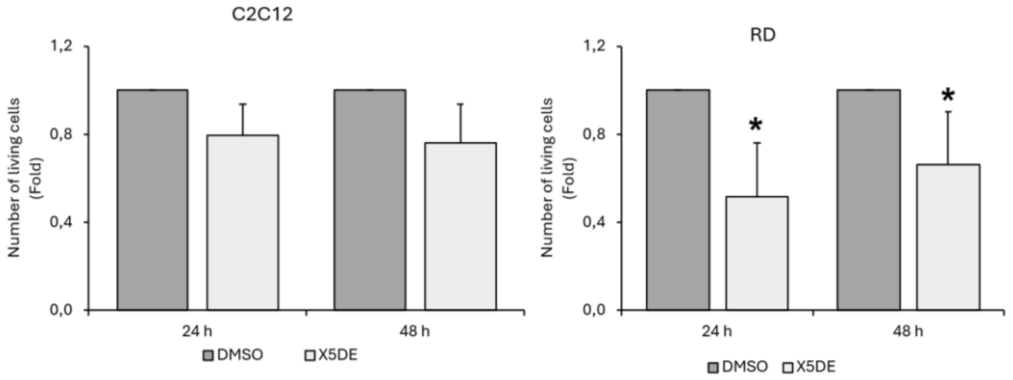

Figure 2. Effect of **X5DE** on the viability of C2C12 myoblasts and RD rhabdomyosarcoma cells. Cells were serum-starved for 24 h and treated with vehicle (DMSO < 0.1%) or **X5DE** (1.0 µM) for 24 or 48 h. Cell viability was determined by the Trypan blue exclusion assay. Data represent mean ± SD from three independent experiments. Statistical significance was evaluated using Student's t-test ($p < 0.05$ vs vehicle-treated control).

Importantly, the proportion of trypan blue-positive cells remained low in both cellular models, indicating preservation of plasma membrane integrity and the absence of extensive acute cytotoxicity. Therefore, the observed decrease in viable RD cells is consistent with a regulated cellular response rather than a generalized loss of membrane integrity or non-specific toxicity.

Xanthone derivatives have been widely investigated as bioactive heterocyclic scaffolds capable of modulating proliferation-associated pathways, oxidative stress responses, and intracellular signaling networks in different biological models.[9,14,15] In this context, the selective response observed for **X5DE** may reflect differences in cellular susceptibility to scaffold-mediated effects. RMS-associated cellular models frequently display alterations in signaling pathways involved in proliferation and survival, including PI3K/Akt-related mechanisms.[18,19]

Interestingly, **A5DE**, despite sharing the same aminoalkyl substitution pattern and displaying Akt-associated activity in skeletal muscle cells,[10] did not reproduce the reduction in RD cell viability observed for **X5DE**. This finding highlights the contribution of scaffold identity to the biological response of this matched xanthone–acridone pair and supports the relevance of heteroatom exchange as a determinant of functional properties in closely related heterocyclic systems.

2.2.2 Preservation of mitochondrial and nuclear morphology after treatment with X5DE and A5DE. To determine whether the viability effects observed after treatment were accompanied by morphological alterations, mitochondrial organization and nuclear morphology were examined by fluorescence microscopy following exposure to **X5DE** and **A5DE**.

Neither compound produced evident changes in mitochondrial network organization or nuclear morphology in C2C12 or RD cells after 24 or 48 h of exposure under the experimental conditions evaluated (Figure 3). Mitochondria maintained a predominantly tubular and interconnected morphology, whereas nuclei remained well defined and showed no evidence of condensation or fragmentation.

 ©AUTHOR(S)

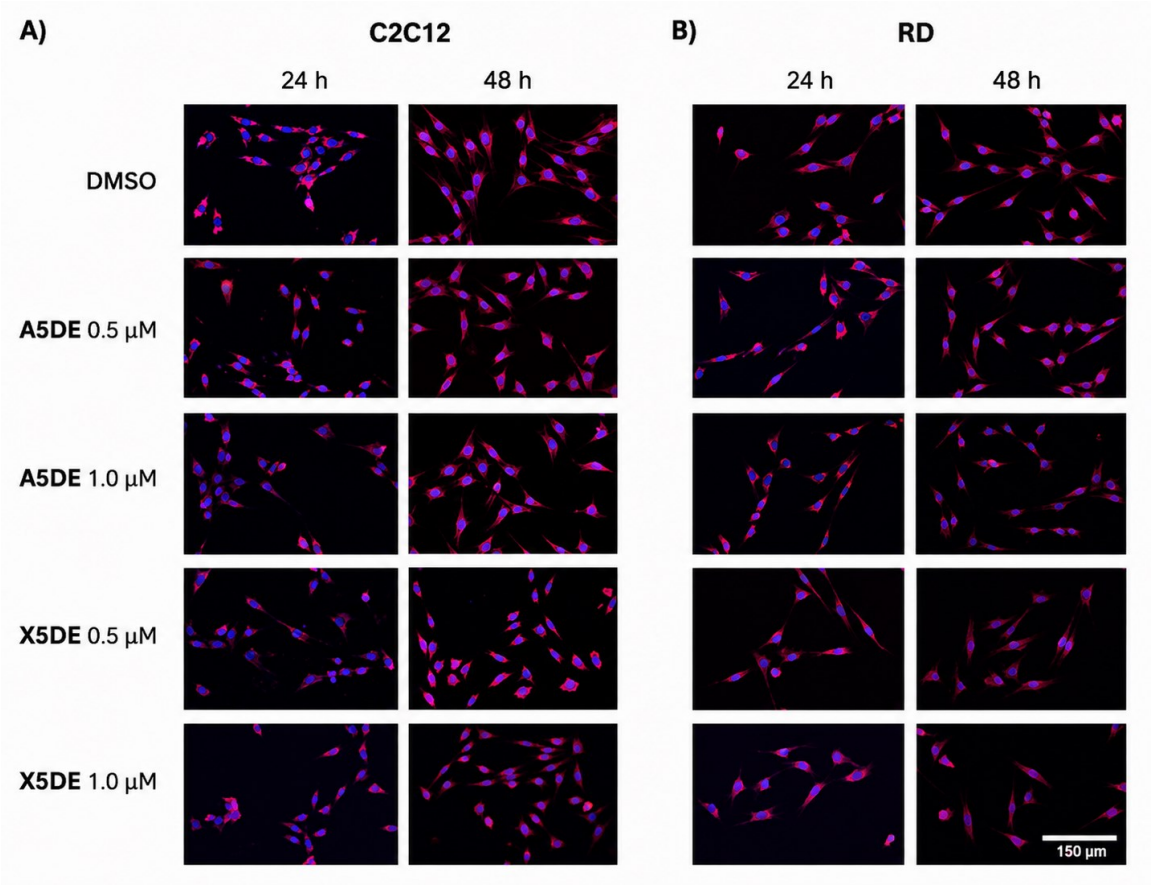

Figure 3. Preservation of mitochondrial and nuclear morphology after treatment with **X5DE** and **A5DE**. Representative fluorescence micrographs of C2C12 myoblasts and RD rhabdomyosarcoma cells serum-starved for 24 h and treated with vehicle, **X5DE** or **A5DE** (0.5 and 1.0 µM) for 24 and 48 h. Mitochondria were stained with MitoTracker Red CMXRos and nuclei were counterstained with DAPI. Images were acquired using a 40× objective. Representative fields from three independent experiments are shown.

Mitochondrial morphology is closely associated with cellular metabolism and stress responses, whereas nuclear condensation and fragmentation are well-established morphological hallmarks of apoptosis.[20–22] The preservation of both mitochondrial organization and nuclear morphology indicates that treatment with **X5DE** or **A5DE** did not induce overt structural damage under the experimental conditions evaluated.

Together with the Trypan blue exclusion results, these findings suggest that the reduction in RD cell viability induced by **X5DE** occurs in the absence of major alterations in mitochondrial or nuclear morphology. This observation supports the concept that subtle scaffold-dependent effects may modulate specific cellular responses without promoting generalized morphological damage.

2.2.3 Comparative modulation of Akt signaling by matched xanthone and acridone scaffolds

Given the central role of PI3K/Akt signaling in skeletal muscle physiology and rhabdomyosarcoma-associated cellular responses, the effects of **X5DE** on Akt phosphorylation were examined in C2C12 and RD cells (Figures 4 and 5). Akt represents a key signaling node regulating cell survival, metabolism, and growth-related processes, and alterations in this pathway have been associated with tumor progression and therapeutic response.[18,19]

 ©AUTHOR(S)

The matched-scaffold design allowed direct evaluation of the influence of heteroatom exchange on Akt signaling while minimizing the contribution of peripheral structural differences.

In C2C12 myoblasts, **X5DE** significantly reduced Akt phosphorylation at Ser473 after both 24 and 48 h of treatment (Figure 4). A similar inhibitory response was previously reported for aminoalkylated acridone derivatives developed by our group, including **A5DE**.[10] These findings indicate that heteroatom exchange does not abolish the ability of either scaffold to modulate Akt phosphorylation, although differences in the magnitude of the response were observed.

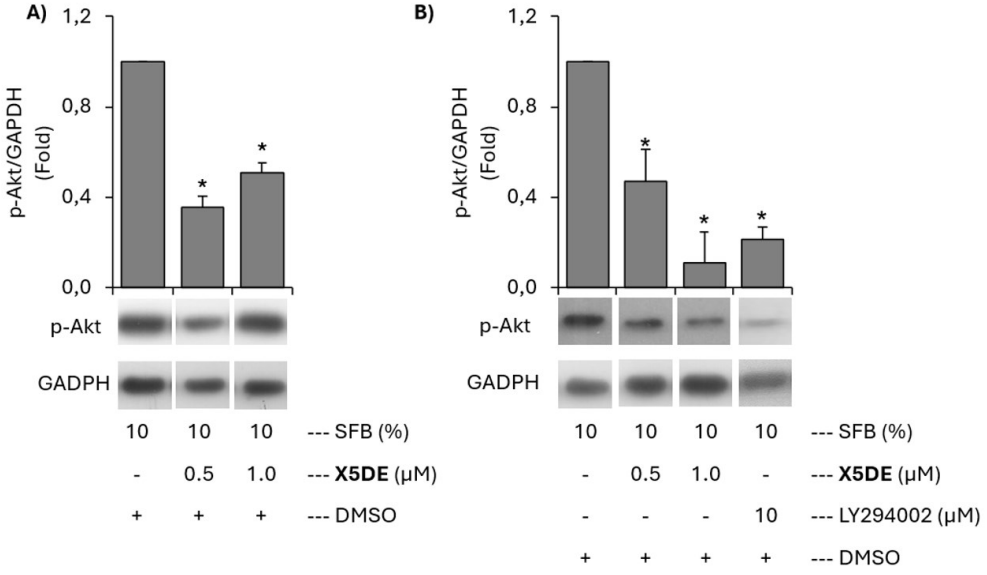

Figure 4. Effect of **X5DE** on Akt phosphorylation in C2C12 myoblasts. Representative immunoblots showing phospho-Akt (Ser473) and GAPDH after 24 h (A) and 48 h (B) of treatment with **X5DE** (1.0 µM). Densitometric quantification of phospho-Akt levels was normalized to GAPDH and expressed as fold change relative to vehicle-treated controls. Data represent mean ± SD from three independent experiments. Statistical significance was evaluated compared with vehicle-treated controls (*$p < 0.05$).

A similar trend was observed in RD rhabdomyosarcoma cells, where **X5DE** produced a reproducible decrease in Akt phosphorylation after 24 h of treatment (Figure 5). However, greater variability was observed at 48 h, which may reflect the complex regulation and adaptive responses commonly associated with PI3K/Akt signaling networks.[18,19] Comparable effects on Akt phosphorylation were previously reported for **A5DE**, indicating that modulation of this pathway is conserved across both scaffold families despite their distinct heteroatom composition.

 ©AUTHOR(S)

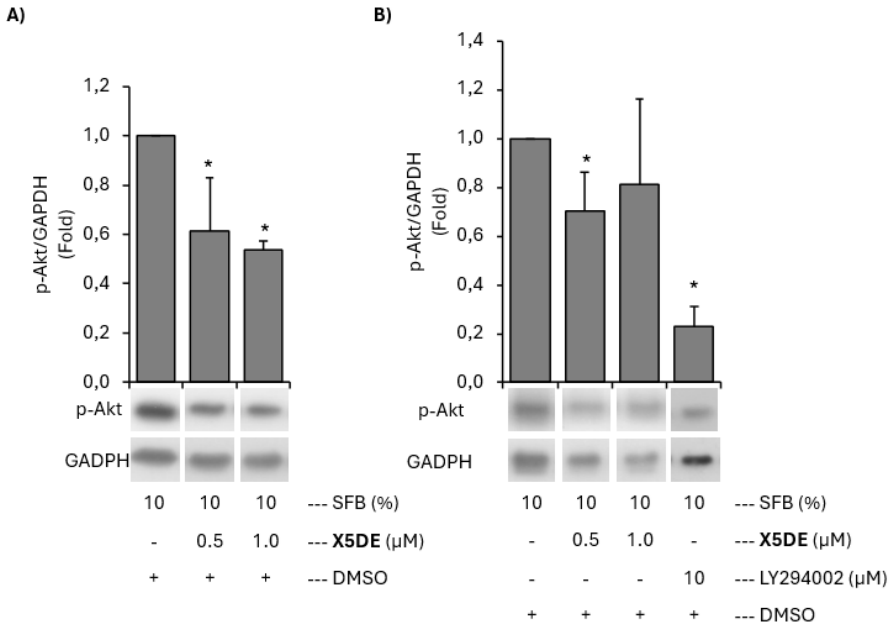

Figure 5. Effect of **X5DE** on Akt phosphorylation in RD rhabdomyosarcoma cells. Representative immunoblots showing phospho-Akt (Ser473) and GAPDH after 24 h (A) and 48 h (B) of treatment with **X5DE** (1.0 μM). Densitometric quantification of phospho-Akt levels was normalized to GAPDH and expressed as fold change relative to vehicle-treated controls. Data represent mean ± SD from three independent experiments. Statistical significance was evaluated compared with vehicle-treated controls (*$p < 0.05$).

To facilitate comparison between the two scaffold families, Akt inhibition values obtained for **X5DE** in the present study and previously reported for **A5DE** are summarized in Table 1.

Table 1. Comparative effects of **X5DE** and **A5DE** on Akt phosphorylation in C2C12 and RD cells

Cell Line	C2C12		RD	
Conditions	24 h	48 h	24 h	48 h
	Inhibition (% ± DE)		Inhibition (% ± DE)	
X5DE 0.5 μM	64.3 ± 4.9	53.0 ± 14.5	38.5 ± 21.2	29.6 ± 15.9
X5DE 1.0 μM	48.8 ± 3.9	88.6 ± 13.3	46.2 ± 3.5	18.6 ± 34.7
A5DE 0.5 μM	85.5 ± 2.9	85.3 ± 4.5	56.8 ± 3.5	28.4 ± 10.5
A5DE 1.0 μM	81.0 ± 10.8	58.9 ± 1.5	51.3 ± 48.7	80.5 ± 1.7
LY294002 10.0 μM	---------	78.3 ± 4.7	---------	76.8 ± 8.4

Percentage of Akt inhibition was calculated relative to vehicle-treated (DMSO) controls under the corresponding experimental conditions. Values are expressed as mean ± SD. **X5DE** data were obtained from the present study, whereas **A5DE** values were taken from a previous report.[10]

 ©**AUTHOR(S)**

Several conclusions emerge from this comparative analysis. First, both derivatives modulate Akt phosphorylation despite differing in the identity of the endocyclic heteroatom. Second, **A5DE** produced a greater reduction in Akt phosphorylation under the previously reported experimental conditions, particularly in C2C12 cells, where inhibition exceeded 80%.[10] Third, the magnitude of Akt inhibition did not directly correlate with the phenotypic responses observed in the viability assays.

Indeed, although **A5DE** consistently reduced Akt phosphorylation, it did not reproduce the reduction in RD cell viability observed for **X5DE**. Conversely, **X5DE** displayed a comparatively moderate effect on Akt-associated signaling while producing a more pronounced impact on cellular viability. These observations indicate that Akt modulation alone is insufficient to explain the divergent biological responses observed between these matched heterocyclic derivatives.

From a structure–response perspective, these results illustrate that closely related heterocyclic systems may influence a common signaling pathway while producing distinct cellular outcomes. Because **X5DE** and **A5DE** differ only in the identity of the endocyclic heteroatom, the observed differences are likely associated with intrinsic scaffold properties, including electronic distribution, hydrogen-bonding capacity, and related molecular interactions.

Overall, these results demonstrate that modulation of Akt signaling alone does not account for the distinct biological profiles of **X5DE** and **A5DE**. Instead, the matched-scaffold analysis supports the concept that heteroatom exchange influences cellular responses beyond a single signaling pathway, highlighting the relevance of scaffold editing as a strategy for tuning the biological properties of closely related heterocyclic systems.

2.2.4 Limited modulation of ERK1/2 signaling by X5DE. To assess whether modulation of MAPK/ERK signaling contributed to the biological responses observed for **X5DE** and **A5DE**, ERK1/2 phosphorylation was evaluated in C2C12 and RD cells (Figures 6 and 7). The MAPK/ERK pathway constitutes another major signaling cascade regulating proliferation, differentiation, survival, and cellular adaptation.[23,24]

In C2C12 myoblasts, **X5DE** produced a modest reduction in ERK1/2 phosphorylation after 24 h of treatment, although this effect was not consistently maintained at 48 h (Figure 6).

 ©AUTHOR(S)

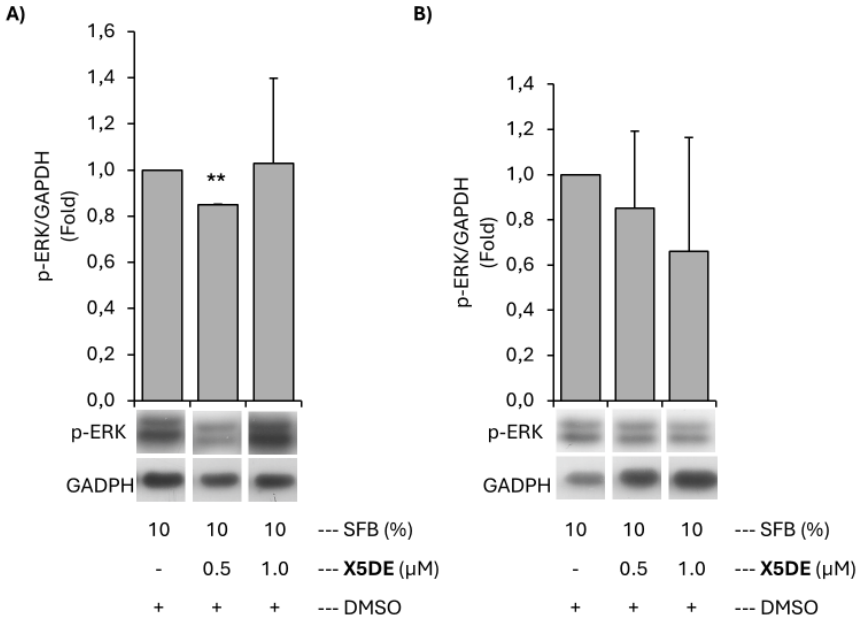

Figure 6. Effect of **X5DE** on ERK1/2 phosphorylation in C2C12 myoblasts. Representative immunoblots showing phospho-ERK1/2, and GAPDH after 24 h (A) and 48 h (B) of treatment with **X5DE** (1.0 µM). Densitometric quantification of phospho-ERK1/2 levels was normalized to GAPDH and expressed relative to vehicle-treated controls. Data represent mean ± SD from three independent experiments.

In RD rhabdomyosarcoma cells, ERK1/2 phosphorylation remained largely unchanged throughout the experimental period (Figure 7).

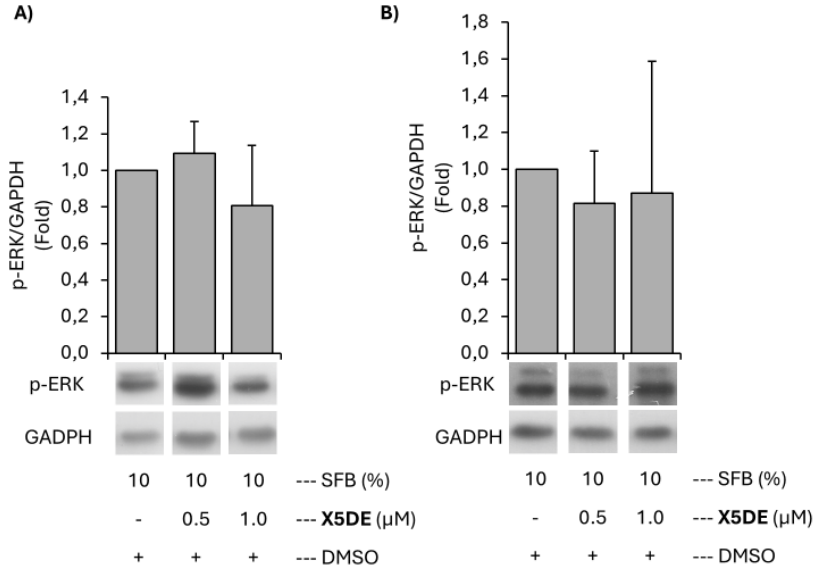

Figure 7. Effect of **X5DE** on ERK1/2 phosphorylation in RD rhabdomyosarcoma cells. Representative immunoblots showing phospho-ERK1/2, and GAPDH after 24 h (A) and 48 h (B) of treatment with **X5DE** (1.0 µM). Densitometric quantification of phospho-ERK1/2 levels was normalized to GAPDH and expressed relative to vehicle-treated controls. Data represent mean ± SD from three independent experiments.

 ©AUTHOR(S)

The limited and transient nature of these responses contrasts with the more consistent effects observed on Akt phosphorylation. Considering the dynamic and context-dependent regulation of MAPK/ERK signaling networks, transient changes in phosphorylation status should be interpreted cautiously.[23,24]

Collectively, these results indicate that ERK1/2 modulation is unlikely to represent a major determinant of the biological responses elicited by **X5DE**. When considered together with the Akt phosphorylation data, the findings suggest that the distinct cellular profiles of **X5DE** and **A5DE** cannot be attributed to modulation of a single signaling pathway. Instead, they support the view that scaffold-dependent molecular features associated with heteroatom exchange contribute to the differential biological behavior of these matched heterocyclic derivatives.

2.2.5 Scaffold-dependent modulation of cell migration. Cell migration was evaluated using wound-healing assays in C2C12 and RD cells following treatment with **X5DE** and **A5DE** (Figures 8 and 9). This experimental approach was employed to determine whether the distinct biological profiles displayed by both matched heterocyclic scaffolds extended to the regulation of cellular motility.

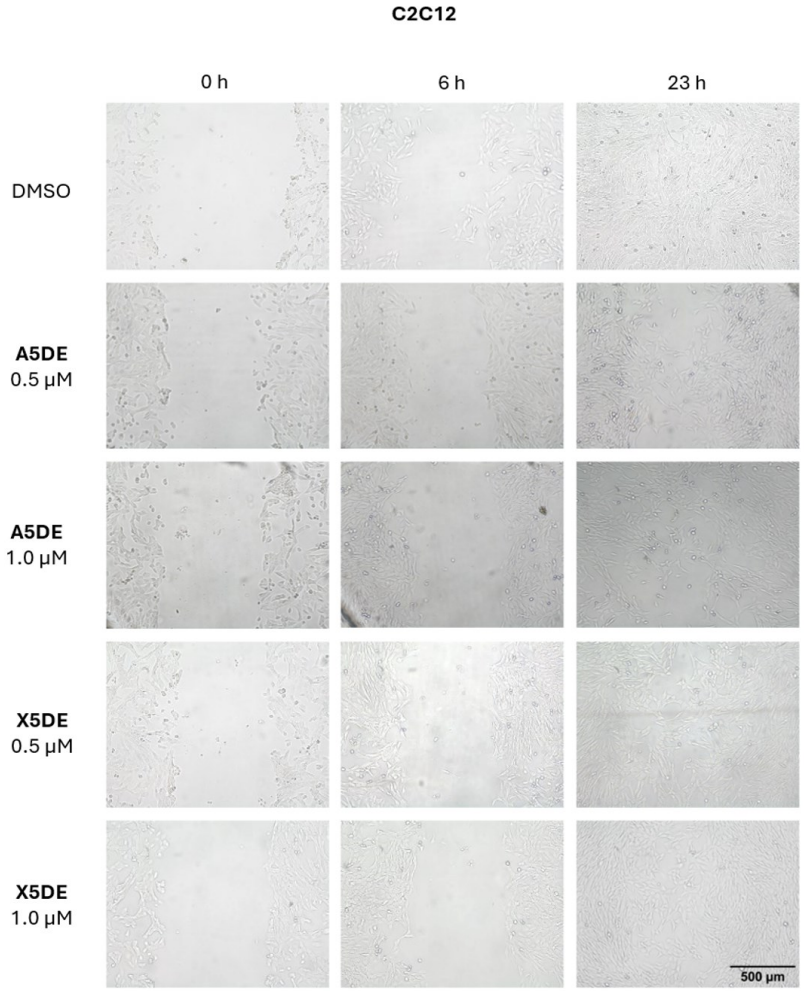

Figure 8. Effect of **X5DE** and **A5DE** on migration of C2C12 myoblasts. Representative phase-contrast micrographs of scratch wound-healing assays performed with C2C12 myoblasts treated with **X5DE** or **A5DE** (0.5 and 1.0 µM). Images were acquired immediately after scratch generation (0 h) and after 6 and 23 h of incubation using a 20× objective. Representative images from three independent experiments are shown.

 ©AUTHOR(S)

In C2C12 myoblasts, both **X5DE** and **A5DE** reduced wound closure capacity, although **A5DE** produced a more pronounced effect under the evaluated conditions (Figure 8).

In RD rhabdomyosarcoma cells, both compounds also affected migratory behavior, although differences in the extent of wound closure revealed distinct responses associated with the xanthone and acridone scaffolds (Figure 9).

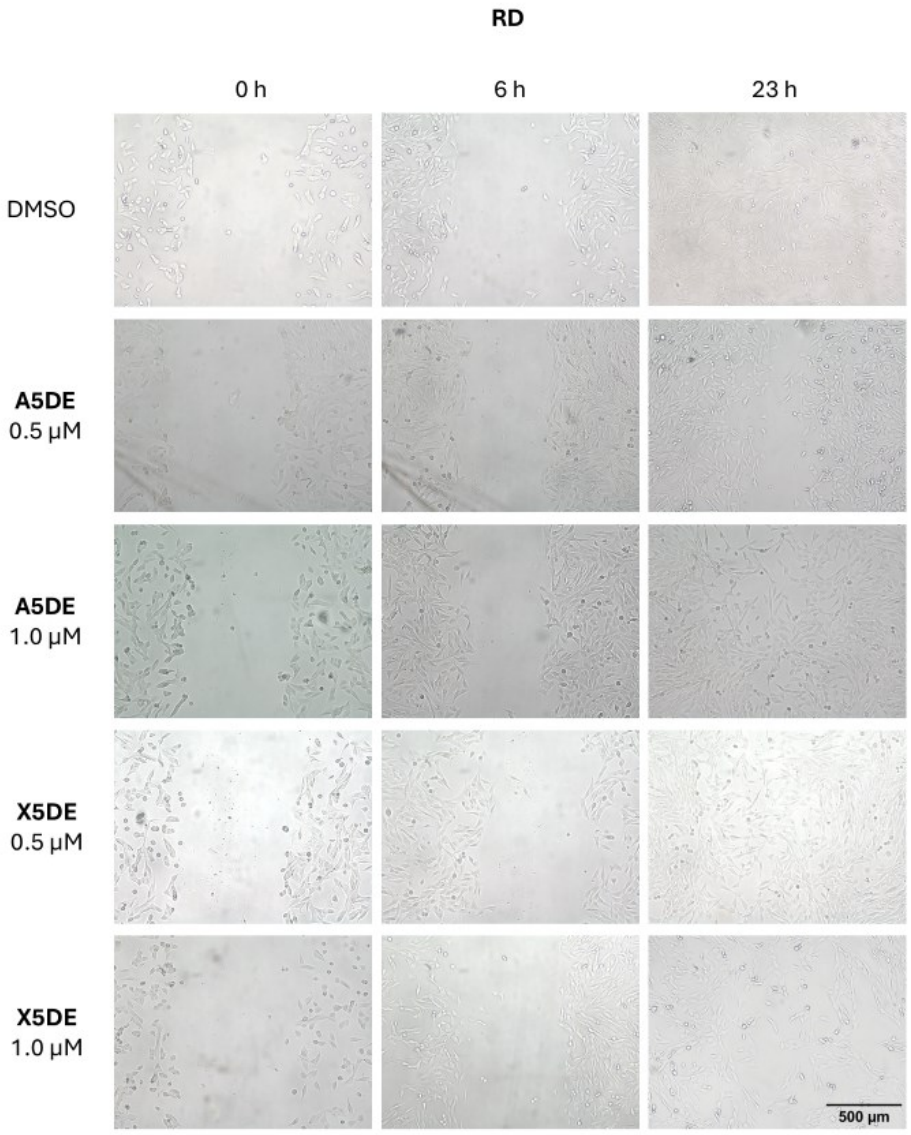

Figure 9. Effect of **X5DE** and **A5DE** on migration of RD rhabdomyosarcoma cells. Representative phase-contrast micrographs of scratch wound-healing assays performed with RD rhabdomyosarcoma cells treated with **X5DE** or **A5DE** under the indicated experimental conditions. Images were acquired immediately after scratch generation (0 h) and after 6 and 23 h of incubation using a 20× objective. Representative images from three independent experiments are shown.

The reduction in migratory capacity occurred in the absence of detectable alterations in mitochondrial organization, nuclear morphology, or plasma membrane integrity. Together with the viability and fluorescence

 ©AUTHOR(S)

microscopy analyses, these observations indicate that the impaired migratory behavior is unlikely to result from nonspecific cytotoxic effects and instead reflects modulation of cellular processes involved in motility.

Given the reported involvement of Akt signaling in cytoskeletal remodeling, cell adhesion, and migratory processes, the observed effects may be considered in the context of Akt modulation together with other scaffold-dependent factors.[25] However, the magnitude of migration impairment did not directly parallel either the extent of Akt inhibition or the viability responses observed in RD cells, suggesting that the biological differences between **X5DE** and **A5DE** cannot be explained by modulation of a single signaling pathway.

Viewed collectively, the present findings reinforce the central premise of the present study: structurally matched xanthone and acridone derivatives, differing only in the identity of the endocyclic heteroatom, produce distinct phenotypic responses despite sharing identical aminoalkyl substitution patterns. Rather than supporting a single mechanism of action, the results indicate that heteroatom exchange within the tricyclic scaffold influences multiple cellular processes, including cell viability, intracellular signaling, and migration. These observations further support scaffold editing as a useful medicinal chemistry strategy for modulating the biological properties of closely related heterocyclic systems.

2.2.6 Scaffold-dependent effects and structure–response considerations. The matched molecular design employed in the present study enabled direct comparison between two closely related heterocyclic systems while minimizing the influence of peripheral structural variation. By maintaining identical aminoalkyl substitution patterns and linker architecture, the biological differences observed between **X5DE** and **A5DE** can be primarily attributed to the identity of the tricyclic heterocyclic scaffold.

Replacement of the endocyclic oxygen atom of the xanthone framework by the corresponding NH group of the acridone scaffold modifies hydrogen-bonding capacity, electronic distribution, polarity, and protonation behavior while preserving the overall molecular topology.[1–6] Such physicochemical differences are likely to influence molecular recognition processes and may ultimately contribute to distinct biological responses.

The experimental findings obtained in the present study are consistent with this interpretation. Although both matched derivatives modulated Akt-associated signaling, only **X5DE** produced a selective reduction in RD cell viability while preserving mitochondrial and nuclear morphology. Likewise, differences in cell migration were observed despite the close structural similarity between the two compounds. These observations indicate that modulation of Akt phosphorylation alone is insufficient to account for the distinct phenotypic profiles associated with each scaffold and suggest that additional scaffold-dependent molecular features contribute to their biological behavior.

It should be emphasized that the present study is based on a representative matched molecular pair and is not intended to establish generalized structure–activity relationships across the xanthone or acridone families. Rather, the objective was to evaluate the consequences of a single scaffold-editing event within a rigorously controlled molecular framework in which peripheral structural variables were deliberately minimized.

Collectively, the present findings demonstrate that heteroatom exchange within closely related tricyclic heteroaromatic systems can produce measurable differences in biological behavior while maintaining essentially unchanged molecular architecture. From a medicinal chemistry perspective, this matched xanthone–acridone comparison further supports scaffold editing as a valuable strategy for modulating the biological properties of bioactive heterocyclic frameworks.

 ©AUTHOR(S)

3. Conclusions

The present study describes a proof-of-concept matched-scaffold comparison between aminoalkylated xanthone and acridone derivatives designed to evaluate the contribution of heteroatom exchange within closely related tricyclic heteroaromatic scaffolds. By maintaining identical aminoalkyl substitution patterns, linker architecture, and terminal diethylamino functionality, the xanthone derivative **X5DE** and the acridone analogue **A5DE** provided a controlled molecular pair for investigating scaffold-dependent effects.

Despite their high degree of structural similarity, **X5DE** and **A5DE** displayed distinct biological response profiles in rhabdomyosarcoma-associated cellular models. The xanthone derivative produced a reduction in cell viability while preserving mitochondrial and nuclear integrity, whereas the corresponding acridone derivative exhibited a different phenotypic profile despite retaining the ability to modulate Akt-associated signaling.

These findings indicate that the divergent cellular responses observed between both derivatives cannot be solely explained by changes in Akt phosphorylation and support the importance of heterocyclic scaffold identity in determining biological behavior. The replacement of the endocyclic oxygen atom by the corresponding nitrogen functionality therefore represents a defined structural modification capable of influencing cellular responses while preserving the overall molecular framework.

Accordingly, replacement of the endocyclic oxygen atom by the corresponding NH group represents a defined scaffold-editing event capable of modulating cellular responses while preserving the overall molecular architecture.

Rather than establishing a conventional structure–activity relationship based on extensive analogue generation, the present work provides a controlled comparison aimed at understanding the consequences of a single scaffold modification within a matched molecular framework. This matched xanthone–acridone pair therefore constitutes a useful experimental model for investigating structure–response relationships associated with heteroatom exchange. More broadly, the present results highlight scaffold editing as a valuable medicinal chemistry strategy for fine-tuning the biological properties of closely related heterocyclic systems.

4. Experimental Section

4.1. General. All reagents and solvents were obtained from commercial suppliers and used as received unless otherwise stated. The synthesis of the xanthone and acridone derivatives followed procedures previously reported by our group.[9,10] Detailed synthetic procedures and full characterization data of the intermediates and final compounds are provided below, and representative spectra are included in the Supporting Information. Thin-layer chromatography (TLC) was performed on Merck silica gel 60 F_{254} aluminum-backed plates and compounds were visualized under UV irradiation (254 nm) and/or by staining with phosphomolybdic acid. Nuclear magnetic resonance (^{1}H and ^{13}C NMR) spectra were recorded at room temperature on a Bruker Avance ARX-300 spectrometer using $CDCl_3$ or DMSO-d_6 as solvents. Chemical shifts (δ) are reported in ppm relative to the residual solvent signals. Infrared spectra were obtained using a Nicolet Nexus 470 FT-IR instrument. Melting points were determined using a Büchi 510 apparatus and are uncorrected. High-resolution mass spectra (HRMS) were recorded using Thermo Fisher LTQ Orbitrap XL and Finnigan MAT 95 spectrometers. Complete characterization data and representative spectra are provided in the Supporting Information.

 ©AUTHOR(S)

The matched xanthone–acridone derivatives **X5DE** and **A5DE** were prepared following the synthetic methodologies previously reported by our group.[9,10] The hydroxylated precursors **1,3-DHX** and **1,3-DHA** were synthesized according to published procedures and are included here to provide complete experimental support for the synthetic sequences employed in this study.

4.2.1. Xanthone series - Synthesis of 1,3-DHX. A mixture of phosphorus pentoxide (0.90 g, 6.35 mmol) and methanesulfonic acid (15 mL) was heated at 90 °C until complete homogenization. Phloroglucinol (0.38 g, 3.0 mmol) and 2-hydroxybenzoic acid (0.46 g, 3.0 mmol) were subsequently added, and the reaction mixture was maintained at 80 °C for 1 h under an argon atmosphere. After cooling, the mixture was carefully poured into ice-water, resulting in the formation of an orange precipitate. The solid was collected by filtration and purified by flash chromatography (hexane/EtOAc 90:10) to afford **1,3-DHX** as a yellow solid (0.48 g, 70%). mp 255–257 °C. ^{1}H NMR (300 MHz, DMSO-d_6) δ: 6.20 (d, J 2.1 Hz, 1H, Ar-H), 6.38 (d, J 2.1 Hz, 1H, Ar-H), 7.41–7.47 (m, 1H, Ar-H), 7. 58 (dd, 1H, Ar-H), 7.83 (td, J 8.0 Hz, 1H, Ar-H), 8.10 (dd, J 8.0, 1.5 Hz, 1H, Ar-H), 11.10 (s, 1H, OH), 12.80 (s, 1H, OH). ^{13}C NMR (75 MHz, DMSO-d_6) δ: 94.8, 98.9, 102.9, 118.3, 120.5, 125.0, 126.5, 136.3, 156.0, 158.1, 164.3, 165.6, 180.4. IR (KBr) ν_{max} 3327 (O-H), 1654 (C=O), 1610, 1570, 1491, 1470, 1445, 1222, 1163, 1078, 827, 762 cm^{-1}. HRMS (EI) *m/z* calcd for $C_{13}H_8O_4$: 228.0423; found 228.0427. The spectroscopic data were in agreement with those previously reported for 1,3-dihydroxyxanthone.[9]

4.2.2. Synthesis of X5Br. 1,3-DHX (600 mg, 2.4 mmol) and K_2CO_3 (660 mg, 4.8 mmol) were suspended in dry acetone (12 mL) under an argon atmosphere. 1,5-Dibromopentane (3.6 mmol) was added, and the reaction mixture was stirred at room temperature for 24 h. After completion of the reaction, the mixture was diluted with ice-water, promoting precipitation of the crude product. The solid was collected by filtration and purified by flash chromatography using hexane/EtOAc (95:5) as eluent (Rf = 0.55, hexane/EtOAc 80:20) to afford **X5Br** as a yellow solid (452 mg, 50%). mp 130–132 °C. ^{1}H NMR (300 MHz, $CDCl_3$): δ 1.56–1.62 (m, 2H, CH_2), 1.75–1.78 (m, 2H, CH_2), 1.85–1.90 (m, 2H, CH_2), 3.37 (t, J 6.9 Hz, 2H, Br-CH_2), 3.97 (t, J 7.0 Hz, 2H, O-CH_2), 6.23 (d, J 2.2 Hz, 1H, Ar-H), 6.31 (d, J 2.3 Hz, 1H. Ar-H), 7.28–7.34 (m, 2H, Ar-H), 7.61 (ddd, J 7.9 Hz, 1H, Ar-H), 8.15 (dd, J 8.0 Hz, 1H, Ar-H), 12.75 (s, 1H, OH). ^{13}C NMR (75 MHz, $CDCl_3$): δ 24.8, 28.3, 32.5, 33.5, 68.3, 93.3, 97.5, 104.1, 117.7, 124.1, 126.1, 128.0, 135.1, 156.1, 157.8, 163.7, 166.3, 180.9. IR (KBr) ν_{max} 3460 (O-H), 2946, 1661 (C=O), 1609, 1573, 1481, 1296, 1163, 1038, 820 cm^{-1}. HRMS (EI) *m/z* calcd for $C_{18}H_{17}BrO_4$: 376.0310; found 376.0313. The spectroscopic data were consistent with those previously reported.[9]

4.2.3. Synthesis of X5DE. X5Br (377 mg, 1.0 mmol) was dissolved in dry acetone (1 mL) under an argon atmosphere, and diethylamine (2.5 mmol) was added dropwise. The resulting mixture was stirred at room temperature for 24 h. The reaction mixture was poured into ice-water, and the resulting yellow solid was collected by filtration, washed with water, and dried under reduced pressure. The crude product was recrystallized from acetone to afford **X5DE** as a yellow solid (258 mg, 70%). mp 150–151 °C. ^{1}H NMR (300 MHz, $CDCl_3$): δ 1.05 (t, J 7.0 Hz, 6H, CH_3), 1.65–1.69 (m, 4H, CH_2), 1.80–1.85 (m, 2H, CH_2), 2.54–2.61 (m, 6H, N-CH_2 and N-CH_2CH_3), 4.08 (t, J 7.1 Hz, 2H, O-CH_2), 6.34 (d, J 2.2 Hz, 1H, Ar–H), 6.42 (d, J 2.2 Hz, 1H, Ar–H), 7.36–7.44 (m, 2H, Ar-H), 7.70-7.75 (m, 1H, Ar-H), 8.24-8.27 (m, 1H, Ar-H), 12.86 (s, 1H, OH). ^{13}C NMR (75 MHz, $CDCl_3$): δ 12.7, 24.3, 27.1, 28.4, 47.1, 54.0, 68.3, 93.9, 99.8, 107.1, 118.2, 121.3, 124.1, 126.6, 135.1, 155.5, 158.5, 162.7, 166.5, 180.9. IR (film) ν_{max} 3440 (O-H), 2964, 2790, 1660 (C=O), 1603, 1571, 1472, 1329, 1298, 1179, 1079, 821, 758 cm^{-1}. HRMS (EI) *m/z* calcd for $C_{22}H_{27}NO_4$: 369.1940; found 369.1944. The spectroscopic data were consistent with those previously reported.[9]

4.2.4 Acridone series - Synthesis of 1,3-DHA. Anthranilic acid (6.85 g, 50 mmol), phloroglucinol (6.85 g, 50 mmol), and anhydrous $ZnCl_2$ (7.0 g, 51 mmol) were suspended in n-butanol (150 mL) under an argon atmosphere and heated under reflux for 24 h. After cooling to room temperature, the reaction mixture was

 ©AUTHOR(S)

diluted with a benzene/water mixture (1:1). The organic phase was separated, dried over anhydrous Na_2SO_4, and concentrated under reduced pressure. The resulting residue was dissolved in hot aqueous NaOH (5%) and filtered. Acidification of the filtrate with dilute H_2SO_4 (5%) promoted formation of the crude acridone derivative, which was purified by flash chromatography (hexane/EtOAc 50:50) as eluent (Rf = 0.30, hexane/EtOAc 50:50) to afford **1,3-DHA** as a yellow solid (7.95 g, 70%). mp >300 °C. ^{1}H NMR (300 MHz, DMSO-d_6): δ 6.04 (d, J 1.2 Hz, 1H, Ar–H), 6.26 (d, J 0.6 Hz, 1H, Ar–H), 7.22 (t, J 7.5 Hz, 1H, Ar–H), 7.43 (d, J 9.0 Hz, 1H, Ar–H), 7.68 (t, J 7.8, 7.2 Hz, 1H, Ar–H), 8.12 (d, J 8.4 Hz, 1H, Ar–H), 10.55 (s, 1H, NH), 11.72 (s, 1H, OH), 14.28 (s, 1H, OH). ^{13}C NMR (75 MHz, DMSO-d_6): δ 91.8, 96.6, 104.3, 117.8, 119.8, 122.1, 126.0, 134.6, 141.7, 144.3, 164.7, 165.2, 180.9. IR (KBr) ν_{max} 3440 (N–H), 3165, 3076, 1645 (C=O), 1609, 1458, 1183, 827 cm^{-1}. HRMS (EI) *m/z* calcd for $C_{13}H_9NO_3$: 227.0582; found 227.0585. The spectroscopic data were consistent with those previously reported.[10]

4.2.5. Synthesis of A5Br. 1,3-DHA (1.0 g, 4.4 mmol) and K_2CO_3 (1.20 g, 8.8 mmol) were suspended in dry acetone (2 mL) under an argon atmosphere. 1,5-Dibromopentane (8.8 mmol) was added dropwise, and the reaction mixture was heated under reflux for 24 h. After cooling to room temperature, the resulting yellow precipitate was collected by filtration, washed with acetone, and purified by flash chromatography on silica gel using hexane/EtOAc 80:20 as eluent (Rf = 0.49, hexane/EtOAc 80:20) to afford **A5Br** as a pale yellow solid (1.21 g, 73%). mp 195–197 °C. ^{1}H NMR (300 MHz, DMSO-d_6): δ 1.55–1.58 (m, 2H, CH_2), 1.79–1.81 (m, 2H, CH_2), 1.92–1.94 (m, 2H, CH_2), 3.68 (t, J 6.9 Hz, 2H, Br-CH_2), 4.11 (t, J 7.0 Hz, 2H, O-CH_2), 6.18 (d, J 2.3 Hz, 1H, Ar–H), 6.40 (d, J 2.0 Hz, 1H, Ar–H), 7.30 (t, J 7.4 Hz, 1H, Ar–H), 7.51 (d, J 8.4 Hz, 1H, Ar–H), 7.76 (t, J 7.9 Hz, 1H, Ar–H), 8.19 (d, J 8.0 Hz, 1H, Ar–H), 11.99 (s, 1H, NH), 14.24 (s, 1H, OH). ^{13}C NMR (75 MHz, DMSO-d_6): δ 25.3, 28.6, 32.9, 36.1, 68.8, 90.7, 95.8, 104.97, 118.0, 119.9, 122.5, 126.1, 135.1, 141.8, 144.2, 164.5, 165.7, 181.3. IR (KBr) ν_{max} 3443 (N–H), 2961, 1654 (C=O), 1620, 1472, 1173, 818 cm^{-1}. HRMS (EI) *m/z* calcd for $C_{18}H_{18}BrNO_3$: 375.0470; found 375.0473. The spectroscopic data were consistent with those previously reported.[10]

4.2.6. Synthesis of A5DE. A5Br (1.0 mmol) was reacted with diethylamine (2.5 mmol) under an argon atmosphere. The resulting mixture was stirred at room temperature for 24 h. The reaction mixture was diluted with water and extracted with ethyl acetate. The organic layer was separated, dried over anhydrous Na_2SO_4, filtered, and concentrated under reduced pressure. The crude product was recrystallized from acetone to afford **A5DE** as a yellow solid (313 mg, 85%). mp 179–180 °C. ^{1}H NMR (300 MHz, $CDCl_3$): δ 1.05 (t, J 7.0 Hz, 6H, CH_3), 1.44–1.54 (m, 4H, CH_2), 1.73-1.83 (m, 2H, CH_2), 2.46 (t, J 6.0 Hz, 2H, N-CH_2), 2.56-2.59 (m, 4H, N-CH_2CH_3), 4.07 (t, J 7.2 Hz, 2H, O-CH_2), 6.14 (d, J 2.2 Hz, 1H, Ar–H), 6.38 (d, J 2.2 Hz, 1H, Ar–H), 7.27-7.32 (m, 1H, Ar–H), 7.50-7.53 (m, 1H, Ar-H), 7.73-7.78 (m, 1H, Ar-H), 8.16-8.19 (m, 1H, Ar-H), 8.74 (s, 1H, NH), 14.08 (s, 1H, OH). ^{13}C NMR (75 MHz, $CDCl_3$): δ 11.5, 24.1, 26.8, 29.1, 47.1, 53.0, 68.3, 89.9, 95.8, 105.0, 116.2, 120.4, 122.0, 126.5, 133.9, 140.5, 142.9, 164.8, 165.7, 181.5. IR (KBr) ν_{max} 3442 (N–H), 2948, 1651 (C=O), 1450, 1163, 819 cm^{-1}. HRMS (EI) *m/z* calcd for $C_{22}H_{28}N_2O_3$: 368.2100; found 368.2104. The spectroscopic data were consistent with those previously reported.[10]

4.3. Biological assays

4.3.1. Reagents and cell lines. The C2C12 mouse myoblast cell line (CRL-1772) was obtained from ATCC (VA, USA), whereas the RD human rhabdomyosarcoma cell line was provided by the Adolfo Lutz Institute (São Paulo, Brazil). Dulbecco's Modified Eagle's Medium (DMEM; 4500 mg/L glucose, L-glutamine, sodium pyruvate, and phenol red) was purchased from Sigma-Aldrich (MO, USA). Fetal bovine serum (FBS) was obtained from Internegocios S.A. (Córdoba, Argentina). Penicillin/streptomycin and nystatin were used as antimicrobial supplements. Primary antibodies against phospho-Akt (Ser473) and phospho-ERK1/2 were purchased from Cell Signaling Technology (MA, USA). Anti-GAPDH antibodies and HRP-conjugated secondary antibodies were obtained from Santa Cruz Biotechnology (CA, USA). Enhanced chemiluminescence reagents

 ©AUTHOR(S)

were purchased from GE Healthcare. DAPI and MitoTracker® Red CMXRos were obtained from Molecular Probes (Thermo Fisher Scientific).

4.3.2. Cell culture and treatment protocol. Cells were cultured in DMEM supplemented with 10% FBS, 1% penicillin/streptomycin, and 0.5% nystatin, and maintained at 37 °C in a humidified atmosphere containing 95% air and 5% CO_2. When cultures reached 70–80% confluence, cells were serum-starved for 24 h in DMEM containing 1% FBS. Subsequently, cells were treated with **X5DE** or **A5DE** at final concentrations of 0.5 and 1.0 µM for the indicated time periods. Both compounds were dissolved in DMSO, and vehicle controls contained the corresponding final concentration of DMSO (≤0.1%). These experimental conditions were selected based on previous observations obtained for related aminoalkylated heterocyclic derivatives.[10,26]

4.3.3. Cell viability assay. After treatment, cells were washed with PBS, trypsinized, and resuspended in DMEM supplemented with 10% FBS. Cell viability was determined by Trypan Blue exclusion assay. Briefly, cells were incubated with Trypan Blue solution (10% final concentration), and viable and nonviable cells were counted using a Neubauer chamber under light microscopy.

4.3.4. Western blot analysis. Following treatment, cells were washed with cold PBS and lysed in buffer containing protease and phosphatase inhibitors. Protein concentration was determined using the Bradford method.[27] Equal amounts of protein were separated by SDS-PAGE according to Laemmli's protocol[28] and transferred onto PVDF membranes. Membranes were blocked with TBS-Tween containing 5% non-fat milk and incubated with the corresponding primary antibodies followed by HRP-conjugated secondary antibodies. Protein bands were detected using enhanced chemiluminescence, and densitometric analysis was performed using ImageJ software.[29]

4.3.5. Mitochondrial network and nuclear morphology analysis. Cells grown on coverslips were treated as described above and incubated with MitoTracker® Red CMXRos (1:15000 dilution in serum-free DMEM) for 20–30 min. Cells were washed, fixed with 4% paraformaldehyde, permeabilized with 0.1% Triton X-100, and stained with DAPI (1:1000). Images were acquired by fluorescence microscopy and processed using Fiji software.[30]

4.3.6. Wound healing assay. Cell migration was evaluated using a wound healing assay. A scratch was generated in confluent monolayers using a sterile pipette tip. After washing with PBS to remove detached cells, cells were treated with **X5DE** or **A5DE**. Migration was monitored over 23 h, corresponding to the experimental period selected according to previous studies performed in C2C12 and RD cellular models.[31,32] Images were acquired at 0, 6, and 23 h. Wound closure was quantified using ImageJ software,[29] and migration percentage was calculated using the MRI Wound Healing Tool following the reported protocol.[33]

4.3.7. Statistical analysis. Data were normalized relative to vehicle-treated controls and expressed as mean ± SD from three independent experiments. Statistical significance was evaluated using Student's *t*-test. Differences were considered statistically significant when $p < 0.05$.

Acknowledgements

This work was supported by the National Scientific and Technical Research Council (Consejo Nacional de Investigaciones Científicas y Técnicas, CONICET; Grant PIP 10100251) and the National University of the South (Universidad Nacional del Sur, Secretaría General de Ciencia y Tecnología; Grant PGI 24/Q138), Argentina. A.G. gratefully acknowledges CONICET for a doctoral fellowship. C.G.B. and D.C.G. are Research Members of CONICET. A.P.I. is a Research Member of the Comisión de Investigaciones Científicas de la Provincia de Buenos Aires (CIC-PBA).

 ©AUTHOR(S)

Supplementary Material

Copies of the ^{1}H and ^{13}C NMR spectra of the synthetic intermediates and the final compounds **X5DE** and **A5DE** are provided in the Supplementary Material associated with this manuscript.

References

1. Peres, V.; Nagem, T. J.; de Oliveira, F. F. *Phytochemistry* **2000**, *55*, 683–710. https://doi.org/10.1016/s0031-9422(00)00303-4
2. Pinto, M. M. M.; Sousa, M. E.; Nascimento, M. S. J. *Curr. Med. Chem.* **2005**, *12*, 2517–2538. https://doi.org/10.2174/092986705774370691
3. Michael, J. P. *Nat. Prod. Rep.* **2008**, *25*, 166–187. https://doi.org/10.1039/B612168N
4. Michael, J. P. Acridone Alkaloids. In: *The Alkaloids: Chemistry and Biology*; Knölker, H.-J., Ed.; Elsevier, 2017; Vol. 78, pp 1–108. https://doi.org/10.1016/bs.alkal.2017.06.001
5. Patani, G. A.; LaVoie, E. J. *Chem. Rev.* **1996**, *96*, 3147–3176. https://doi.org/10.1021/cr950066q
6. Meanwell, N. A. *J. Med. Chem.* **2011**, *54*, 2529–2591. https://doi.org/10.1021/jm1013693
7. Sousa, M. E.; Pinto, M. M. M. *Curr. Med. Chem.* **2005**, *12*, 2447–2479. https://doi.org/10.2174/092986705774370736
8. Qin, J.; Lan, W.; Liu, Z.; Huang, Z.; Du, L.; Guan, H.; Li, Z.; Chen, Y. *Chem. Cent. J.* **2013**, *7*, 78. https://doi.org/10.1186/1752-153X-7-78
9. Menéndez, C. A.; Biscussi, B.; Accordino, S. R.; Murray, A. P.; Gerbino, D. C.; Appignanesi, G. A. *Bioorg. Chem.* **2017**, *75*, 201–209. https://doi.org/10.1016/j.bioorg.2017.09.012
10. Irazoqui, A. P.; Menéndez, C. A.; Steingruber, H. S.; Gonzalez, A.; Appignanesi, G. A.; Buitrago, C. G.; Gerbino, D. C. *Bioorg. Chem.* **2023**, *130*, 106222. https://doi.org/10.1016/j.bioorg.2022.106222
11. Santra, S.; Sharapov, A. D.; Fatykhov, R. F.; Potapova, A. P.; Khalymbadzha, I. A.; Valieva, M. I.; Kopchuk, D. S.; Zyryanov, G. V.; Bunev, A. S.; Melekhin, V. V.; Gaviko, V. S.; Zonov, A. A. *Pharmaceuticals* **2023**, *16*, 403. https://doi.org/10.3390/ph16030403
12. Georgakopoulos, A.; Kalampaliki, A. D.; Gioti, K.; Hamdoun, S.; Giannopoulou, A. F.; Efferth, T.; Stravopodis, D. J.; Tenta, R.; Marakos, P.; Pouli, N.; Kostakis, I. K. *Arab. J. Chem.* **2020**, *13*, 7953–7969. https://doi.org/10.1016/j.arabjc.2020.09.025
13. Hussain, J.; Rea, C. *J. Chem. Inf. Model.* **2010**, *50*, 339–348. https://doi.org/10.1021/ci900450m
14. Griffen, E.; Leach, A. G.; Robb, G. R.; Warner, D. J. *J. Med. Chem.* **2011**, *54*, 7739–7750. https://doi.org/10.1021/jm200452d
15. Welsch, M. E.; Snyder, S. A.; Stockwell, B. R. *Curr. Opin. Chem. Biol.* **2010**, *14*, 347–361. https://doi.org/10.1016/j.cbpa.2010.02.018
16. 16. Brown, N. *Mol. Inf.* **2014**, *33*, 458–462.

 ©AUTHOR(S)

https://doi.org/10.1002/minf.201400037
17. Strober, W. Trypan Blue Exclusion Test of Cell Viability. *Curr. Protoc. Immunol*. **2015**, 111, A3.B.1–A3.B.3. https://doi.org/10.1002/0471142735.ima03bs111
18. Petricoin, E. F.; Espina, V.; Araujo, R. P.; Midura, B.; Yeung, C.; Wan, X.; Eichler, G. S.; Johann, D. J.; Qualman, S.; Tsokos, M.; Krishnan, K.; Helman, L. J.; Liotta, L. A. *Cancer Res.* **2007**, *67*, 3431–3440. https://doi.org/10.1158/0008-5472.CAN-06-1344
19. Manning, B. D.; Toker, A. *Cell* **2017**, *169*, 381–405. https://doi.org/10.1016/j.cell.2017.04.001
20. Chan, D. C. *Annu. Rev. Pathol*. **2020**, *15*, 235–259. https://doi.org/10.1146/annurev-pathmechdis-012419-032711
21. Bock, F. J.; Tait, S. W. G. *Nat. Rev. Mol. Cell Biol*. **2020**, *21*, 85–100. https://doi.org/10.1038/s41580-019-0173-8
22. Galluzzi, L.; Vitale, I.; Aaronson, S. A.; Abrams, J. M.; Adam, D.; Agostinis, P.; Alnemri, E. S.; Altucci, L.; Amelio, I.; Andrews, D. W.; et al. 2018. *Cell Death Differ*. **2018,** *25*, 486–541. https://doi.org/10.1038/s41418-017-0012-4
23. Plotnikov, A.; Zehorai, E.; Procaccia, S.; Seger, R. *Biochim. Biophys. Acta* **2011**, *1813,* 1619–1633. https://doi.org/10.1016/j.bbamcr.2010.12.012
24. Lavoie, H.; Gagnon, J.; Therrien, M. *Nat. Rev. Mol. Cell Biol*. **2020**, *21*, 607–632. https://doi.org/10.1038/s41580-020-0255-7
25. Xue, G.; Hemmings, B. A. *J. Nat.l Cancer Inst.* **2013**, *105*, 393–404. https://doi.org/10.1093/jnci/djs648
26. Orzechowski, A.; Grzelkowska, K.; Karlik, W. *Basic Appl. Myol*. **2001**, *11*, 31–44.
27. Bradford, M. M. *Anal. Biochem*. **1976**, *72*, 248–254. https://doi.org/10.1016/0003-2697(76)90527-3
28. Laemmli, U. K. *Nature* **1970**, *227*, 680–685. https://doi.org/10.1038/227680a0
29. Schneider, C. A.; Rasband, W. S.; Eliceiri, K. W. *Nat. Methods* **2012**, *9*, 671–675. https://doi.org/10.1038/nmeth.2089
30. Schindelin, J.; Arganda-Carreras, I.; Frise, E.; Kaynig, V.; Longair, M.; Pietzsch, T.; Preibisch, S.; Rueden, C.; Saalfeld, S.; Schmid, B.; Tinevez, J.-Y.; White, D. J.; Hartenstein, V.; Eliceiri, K.; Tomancak, P.; Cardona, A *Nat. Methods* **2012**, *9*, 676–682. https://doi.org/10.1038/nmeth.2019
31. Irazoqui, A. P.; Boland, R. L.; Buitrago, C. G. *J. Mol. Endocrinol*. **2014**, *53,* 331–343. https://doi.org/10.1530/jme-14-0102
32. Irazoqui, A. P.; Gonzalez, A.; Buitrago, C. G. *J. Steroid Biochem. Mol. Biol*. **2022**, *222*, 106146. https://doi.org/10.1016/j.jsbmb.2022.106146
33. Instituto de Investigaciones Biomédicas "Alberto Sols". Protocolo de Ensayo de Herida. **2013**, 1–14.

This paper is an open access article distributed under the terms of the Creative Commons Attribution (CC BY) license (http://creativecommons.org/licenses/by/4.0/)